Electronic Supplementary Material (ESI) for Nanoscale.

Supporting Information

Arrays of High Quality SAM-Based Junctions and their Application in Molecular Diode Based Logic

Albert Wan[1], *C. S. Suchand Sangeeth* [1], *Lejia Wang*[1], *Li Yuan*[1], *Li Jiang*[1] *and Christian A. Nijhuis*[1,2,3]*

[1]Department of Chemistry, National University of Singapore, 3 Science Drive, Singapore 117543

[2]Solar Energy Research Institute of Singapore (SERIS), 7 Engineering Drive 1, National University of Singapore, Singapore 117574, Singapore

[3]Graphene Research Centre, National University of Singapore, 2 Science Drive 3, Singapore 117542, Singapore.

Corresponding author:

E-mail: chmnca@nus.edu.sg

Synthesis

Scheme 1. Synthetic route to prepare $HSCH_2PhCCPh(CH_2)_3Fc$.

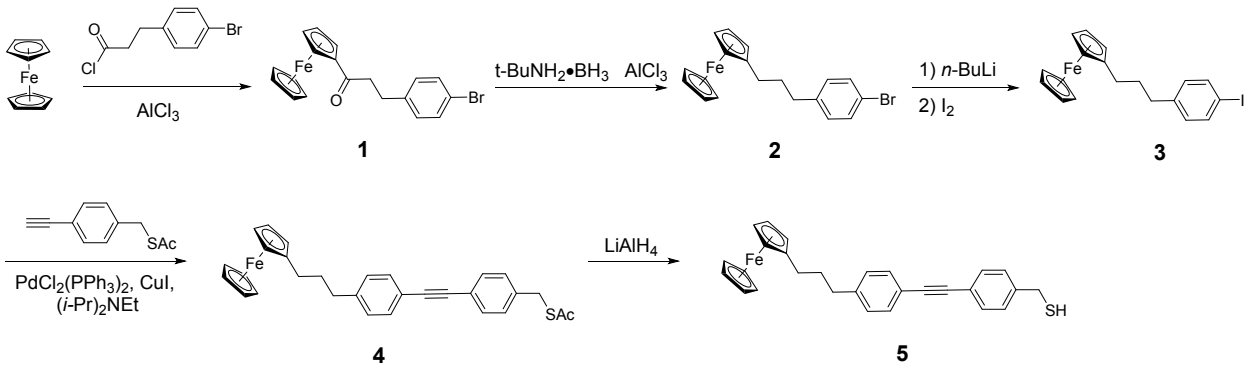

General Procedures:

The bis(triphenylphosphine)palladium(II) chloride, copper(I) iodide, N-ethyldiisopropylamine, 3-(4-bromophenyl)propanoic acid, oxalyl chloride, borane-tert-butylamine complex and n-butyllithium (2.5M in hexane) were purchased from Alfa Aesar. Ferrocene, anhydrous aluminum chloride, lithium aluminum hydride, iodine were purchased from Sigma-Aldrich. Chemicals were used without further purification. Solvents for chemical synthesis were freshly distilled prior to use. Dichloromethane was distilled from calcium chloride and THF was distilled from sodium/benzophenone. Deionized water (18.2 MΩcm) was generated from a water purifier (Purelab Option). All moisture sensitive reactions were performed under a N_2-atmosphere. Thin layer chromatography (TLC) glass plates coated with 0.25 mm thickness of silica gel 60 and fluorescent indication UV_{254} (Macherey-Nagel) were used to monitor the progress of the reactions. The products were purified by column chromatography over silica gel (pore size 60 Å, 230-400 mesh particle size, 40-63 μm particle size, Sigma-Aldrich). ^1H and ^{13}C NMR spectra were recorded on a Bruker Avance 300 MHz (AV300) spectrometer using chloroform-d as a solvent. Electrospray ionization (ESI) high resolution mass spectra were recorded on a Finnigan LCQ mass spectrometer.

Compound 1 3-(4-bromophenyl)propanoyl chloride was prepared from 3-(4-bromophenyl)propanoic acid. Oxalyl chloride (1.6 mL, 18 mmol) was added to a stirred solution of 3-(4-bromophenyl)propanoic acid (2.75 g, 12 mmol) in anhydrous dichloromethane (20 mL) at 0 °C. DMF (10 μl, 0.1 mmol) was then added and the reaction mixture stirred for 30 min at 0 °C. The flask was warmed to room temperature and stirred for 1 hour. The solvent was removed under reduced pressure to yield 3-(4-bromophenyl)propanoyl chloride as a crude yellow solid which was used immediately and without purification in the next step. In a 100 ml Schlenk flask, ferrocene (2 g, 10.8 mmol) and anhydrous $AlCl_3$ (2 g, 14 mmol) were dissolved in anhydrous dichloromethane (25 mL), next a solution of 3-(4-bromophenyl)propanoyl chloride in anhydrous dichloromethane (25 mL) was added to the reaction mixture dropwise at 0 °C. The reaction mixture was stirred for 2 h at 0 °C under a nitrogen atmosphere. After addition of deionized water (30 mL), the reaction mixture was stirred for an additional 10 min. The dark red colored organic layer was separated from the blue colored aqueous layer. The aqueous layer was extracted three times with dichloromethane (25 mL) and the combined organic layers were washed with saturated sodium chloride, dried over sodium sulfate, filtered, and concentrated using rotary evaporation. The crude product was purified by column chromatography (hexane/DCM = 1:1) to yield the product (2.9 g, 73% yield) as a red solid. ^{1}H NMR ($CDCl_3$, 300 MHz) δ 7.42 (d, 2H, J=8.1 Hz), 7.17 (d, 2H, J=8.1 Hz), 4.76 (s, 2H), 4.49 (s, 2H), 4.05 (s, 5H), 3.00 (s, 4H); ^{13}C NMR ($CDCl_3$, 75 MHz) δ 202.7, 140.6, 131.5, 130.4, 119.9, 78.8, 76.6, 69.7, 69.2, 41.1, 29.4; ESI HRMS *m/z* calcd for $C_{19}H_{18}FeBrO$ 396.9886, found 396.9893 (M^++H)

Compound 2 Borane–tert-butylamine complex (3.8 g, 43.8 mmol) in anhydrous dichloromethane (50 mL) was added at 0 °C to a suspension of $AlCl_3$ (2.92 g, 21.9 mmol) in

anhydrous dichloromethane (50 mL), the resulting mixture was allowed to stir at 0 °C for 1h until a clear solution was obtained. A solution of compound **1** (2.9 g, 7.3 mmol) in anhydrous dichloromethane (25 mL) was added dropwise. The reaction mixture was stirred at 0 °C for 2 h and then hydrolyzed with deionized water (30 mL). The aqueous layer was extracted three times with dichloromethane (25 mL) and the combined organic layers were washed with 0.1 M HCl, water and saturated sodium chloride, dried over sodium sulfate, filtered, and concentrated using rotary evaporation. The crude product was purified by column chromatography (hexane/DCM = 10:1) to provide product (2.6 g, 95% yield) as a yellow solid. ^{1}H NMR ($CDCl_3$, 300 MHz) δ 7.40 (d, 2H, J=8.4 Hz), 7.06 (d, 2H, J=8.4 Hz), 4.08 (s, 5H), 4.05 (s, 4H), 2.59 (t, 2H, J=7.8 Hz), 2.35 (t, 2H, J=7.8 Hz), 1.86-1.76 (m, 2H); ^{13}C NMR ($CDCl_3$, 75 MHz) δ 141.3, 131.3, 130.2, 119.4, 88.7, 68.5, 68.0, 67.1, 35.1, 32.5, 29.0; ESI HRMS *m/z* calcd for $C_{19}H_{19}FeBr$ 382.0016, found 382.0016 (M^+)

Compound 3 A solution of compound **2** (764 mg, 2 mmol) in 25 ml anhydrous THF was cooled to -78 °C under nitrogen atmosphere, n-butyllithium 0.96 ml (2.5 M in hexane) was added dropwise, and the reaction mixture was stirred at -78°C for 30 min. A solution of iodine (660 mg, 2.6 mmol) in 10 mL anhydrous THF was added dropwise. After stirring for 30 min at -78 °C, the reaction mixture was warmed to room temperature and stirred for another 1 h, then the reaction was quenched by deionized water (18.2 MΩcm, 30 mL). The aqueous layer was extracted three times with dichloromethane (25 mL) and the combined organic layers were washed with sodium thiosulfate solution, water and saturated sodium chloride, dried over sodium sulfate, filtered, and concentrated using rotary evaporation. The crude product was purified by column chromatography (hexane/DCM = 10:1) to provide 772 mg of product in 90% yield as a yellow solid. ^{1}H NMR ($CDCl_3$, 300 MHz) δ 7.62 (d, 2H, J=8.1 Hz), 6.95 (d, 2H, J=8.1 Hz),

4.09 (s, 5H), 4.06 (s, 4H), 2.59 (t, 2H, J=7.5 Hz), 2.36 (t, 2H, J=7.5 Hz), 1.87-1.79 (m, 2H); ^{13}C NMR ($CDCl_3$, 75 MHz) δ 142.0, 137.3, 130.5, 90.7, 88.6, 68.5, 68.0, 67.1, 35.1, 32.4, 29.0; ESI HRMS *m/z* calcd for $C_{19}H_{19}FeI$ 429.9875, found 429.9877 (M^+)

Compound 4 Compound **3** (430 mg, 1 mmol), S-(4-ethynylbenzyl) ethanethioate (228 mg, 1.2 mmol), $Pd(PPh_3)_2Cl_2$ (35 mg, 0.05 mmol), and CuI (19 mg, 0.1 mmol) were dissolved in anhydrous THF (15 ml) in a Schlenk tube, then 5 mL N,N-diisopropylethylamine were added. The reaction mixture was deoxygenated using the freeze-pump-thaw method (three cycles). The mixture was then stirred at 50 °C for 5 h with the progress of the reaction being carefully monitored by TLC analysis (hexane/DCM = 1:1). When the reaction was complete, the solvents were removed *in vacuo* and the desired product was isolated by column chromatography (hexane/DCM = 1:1) to provide product (300 mg) in 61% yield as a yellow solid. ^{1}H NMR ($CDCl_3$, 300 MHz) δ 7.45 (brd, 4H, J=8.1 Hz), 7.27(d, 2H, J=8.1 Hz), 7.17 (d, 2H, J=8.4 Hz), 4.12 (s, 5H), 4.09 (brs, 4H), 2.65 (t, 2H, J=7.5 Hz), 2.36(s, 3H), 2.35 (t, 2H, J=7.5 Hz), 1.89-1.79 (m, 2H); ^{13}C NMR ($CDCl_3$, 75 MHz) δ 194.9, 142.9, 137.7, 131.7, 131.6, 128.8, 128.5, 122.4, 120.5, 89.8, 88.5, 88.3, 69.2, 68.7, 67.7, 35.6, 33.3, 32.3, 30.3, 29.0; ESI HRMS *m/z* calcd for $C_{30}H_{29}FeOS$ 493.1283, found 493.1291 (M^++H)

Compound 5 Lithium aluminum hydride (57 mg, 1.5 mmol) was dissolved in anhydrous THF (10 mL) at 0 °C and purged with nitrogen for 10 min. A solution of **4** (246 mg, 0.5 mmol) in anhydrous THF (10 mL) was added dropwise. The resulting mixture was stirred for 20 min at 0 °C and an additional 1 h at room temperature. After re-cooling to 0°C, 3N hydrochloric acid was added until the entire solid dissolved. To the biphasic mixture we added diethyl ether and water. The organic phase was separated and washed with brine, dried over Na_2SO_4, the solvents were

removed *in vacuo* and the desired product was isolated by column chromatography (hexane/DCM = 2:1) to provide the product (180 mg, 80% yield) as a yellow solid. ^{1}H NMR ($CDCl_3$, 300 MHz) δ 7.48 (d, 2H, J=8.1 Hz), 7.46(d, 2H, J=8.1 Hz), 7.30 (d, 2H, J=8.1 Hz), 7.18 (d, 2H, J=8.1 Hz), 4.08 (s, 5H), 4.05 (br, 4H), 3.75 (d, 2H, J=7.2 Hz), 2.66 (t, 2H, J=7.5 Hz), 2.36 (t, 2H, J=7.5 Hz), 1.90-1.82 (m, 2H), 1.77 (t, 1H, J=7.8 Hz); ^{13}C NMR ($CDCl_3$, 75 MHz) δ 142.9, 141.1, 131.8, 131.6, 128.5, 128.1, 122.2, 120.5, 89.7, 88.7, 88.6, 68.5, 68.0, 67.1, 35.6, 32.4, 29.0, 28.8; ESI HRMS *m/z* calcd for $C_{28}H_{26}FeS$ 450.1099, found 450.1105 (M^+).

Electrochemistry. We characterized the SAMs of Au^{TS}-$SCH_2PhCCPh(CH_2)_3Fc$ electrochemically with cyclic voltammetry (CV) (AUTOLAB PGSTA302N; NOVA 1.9 software), and a home-build electrochemical cell with a Pt-disk counter electrode inside. The Ag/AgCl was chosen as a reference electrode and 1.0 M $HClO_4$ solution as the electrolyte. The area (A) of the SAM exposed to the electrolyte was 0.33 cm^2. The whole setup was equipped with a Faraday cage. We used a scan rate of 1.0 V/s and a voltage window from -0.1 to +0.9 V to record the CV data. Three substrates were used to determine the error.

We calculated the surface coverage (Γ_{Fc}, mol/cm^2) of the Fc units with equation S1

$$\Gamma_{Fc} = Q_{tot}/nFA \quad \text{(S1)}$$

where Q_{tot} is the total charge obtained by integration o oxidation wave of the cyclic voltammogram, n is the number of electrons per mole of reaction, and F is the Faraday constant (96485 C/mol). The value of Γ_{Fc} is 4.31±0.15 × 10^{-10} mol/cm^2 which is very close to the theoretical maximum coverage 4.5 × 10^{-10} mol/cm^2.[2] From this observation we conclude that the molecules are standing up and form well-packed monolayers.

We also estimated the highest occupied molecular orbital, E_{HOMO} (eV, relative to vacuum), from the cyclic voltammogram with equation S2

$$E_{HOMO} = E_{abs,NHE} - e\,E_{1/2,NHE} \quad \text{(S2)}$$

where $E_{abs,NHE}$ is the absolute potential energy of the normal hydrogen electrode (-4.5 eV), e is the elementary charge (1.602×10^{-19} C), and $E_{1/2,\ NHE}$ is the formal half-wave potential versus normal hydrogen electrode. We listed all the results in Table S1. The value of E_{HOMO} is -5.03±0.01 eV with respect to the energy level of vacuum (E_{vac} = 0 eV).

Figure S1. The cyclic voltammogram of a SAM of Au^{TS}-$SCH_2PhCCPh(CH_2)_3Fc$ with aqueous 1.0 M $HClO_4$ as the electrolyte solution and Ag/AgCl as the reference electrode recorded at a scan rate of 1.0 V/s.

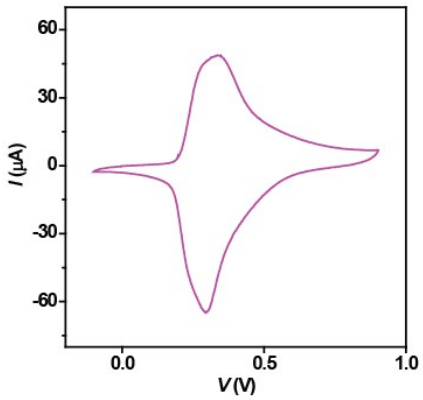

Spectroscopy. We carried out all the X-ray photoelectron spectroscopy (XPS) measurements at the SINS (Surface, Interface and Nanostructure Science) beamline of the Singapore Synchrotron Light Source (SSLS). The experimental procedures of the have been published in the supplementary information of ref 1. We plan to report a detailed characterization of these SAMs elsewhere[2] and therefore we only give the high resolution XPS spectra of S 2*p* and Fe $2p_{3/2}$ of the Au^{TS}-$SCH_2PhCCPh(CH_2)_3Fc$ SAM below. The binding energy (BE, eV) of S 2*p* spectra is

located at about 161.8 eV which is the BE of the Au-S bond. We do not observe any physisorbed molecules (S 2*p* signal at ~163 eV), oxidized sulfur (S 2*p* signal at ~166 eV), or a disordered chemisorbed phase (S 2*p* signal at ~160.5 eV) which indicate the SAMs are of good quality.[1,3]

Figure S2. The high resolution XPS spectra of S 2*p* and Fe $2p_{3/2}$ of the Au^{TS}-$SCH_2PhCCPh(CH_2)_3Fc$ SAM.

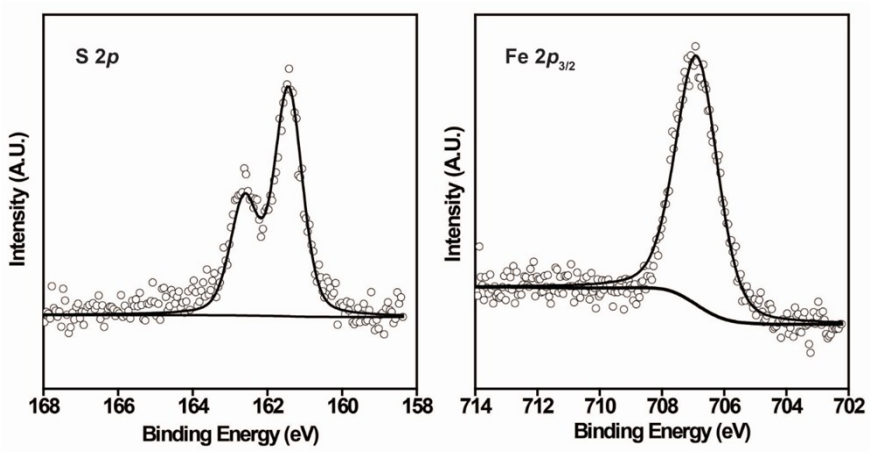

Definition of reproducibility. The reproducibility of electrical measurements of SAM-based junctions can be explained by Figure S3. The precision (σ_{log}) is defined as half of the width of half of the height of the distribution of the measured log|*J*| values at a given bias. The accuracy is defined as the closeness of the value of the measured log|*J*| to its true value or standard value. Figure S3 illustrates that data can be precise, but not accurate, and *vice versa*. A measurement with good reproducibility means the distribution (width) of the data is small (highly precise), and the measured value is close to the reference value (highly accurate).

Figure S3. Schematic diagram of defining reproducibility in terms of precision (σ_{log}) and accuracy for electrical measurements of SAM-based junctions. This diagram is generated following similar diagrams discussed in the references 4 and 5.

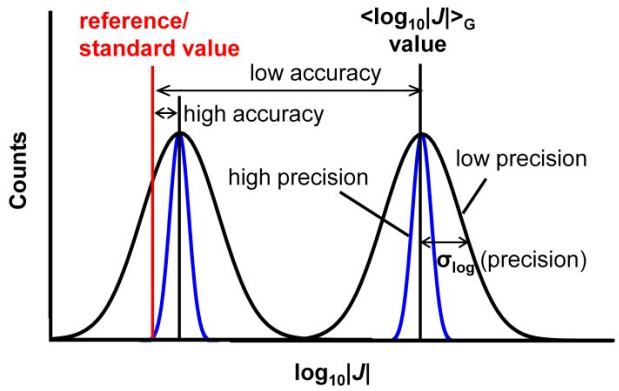

Fabrication of the mold. We fabricated the mold which consists of photoresist lines and pillars on a Si wafer by using a procedure of two-step photolithography reported in the literature.[2,3] We cleaned the wafer by immersing it in a mixture of NH_4OH:H_2O_2:H_2O (1:1:4 volume ratio) at 80 ^oC for 10 minutes followed by exposing the wafer to hexamethyldisilazane (HMDS) vapor in a bake oven (YES 310TA) at 150 ^oC for 5 minutes to improve the adhesion between the photoresist and the wafer. We spin-coated SU8 2010 photoresist at 3500 rpm for 1 minute to form a 10 μm photoresist layer on the wafer (Figure S4a). After baking the substrate at 65 ^oC for 1 minute and at 95 ^oC for 3 minutes, we exposed the photoresist with UV light (5 mW) for 22 seconds through a shadow mask using a mask aligner (Suss Microtech) as shown in Figure S4b. After the post-exposure bake at 65 ^oC for 1 minute and 95 ^oC for 3 minutes, we developed the photoresist in SU8 developer (Microchem) for 2 minutes to form the line structures (Figure S4c). We rinsed the substrate with copious amount of isopropyl alcohol (IPA) to remove the photoresist residues and blew the substrate to dryness with N_2. The substrate was hard-baked at 150 ^oC for 5 minutes, followed by spin-coating (2500 rpm for 1 min) of a 60 μm thick layer of SU8 3050 photoresist at for the second lithography step to generate the pillars (Figure S4d). The substrate was baked at 95 ^oC for 30 minutes, followed by exposure to UV light for 50 seconds through a shadow mask, which was aligned with respect to the wafer using the mask aligner

prior to the exposure (Figure S4e). The substrate was post-exposure baked at 65 °C for 1 minute and at 95 °C for 5 minutes, and then was developed in SU8 developer for 8 minutes to remove the unexposed photoresist (Figure S4f). We rinsed the substrate with IPA and blew the substrate to dryness with N_2, followed by a hard-baked at 150 °C for 5 minutes.

Figure S4. Schematic diagram of the fabrication procedure of the mold: (a) spin-coat a 10 µm thick layer of SU8 2010 photoresist on a Si wafer, (b) Expose the photoresist with UV light through a shadow mask, (c) Remove the unexposed photoresist by developing. (d) Spin-coat a 60 µm thick layer of SU8 3050 on the substrate, (e) Align the shadow mask above the substrate, and then exposed the photoresist with UV light through the mask, and (f) developed the photoresist.

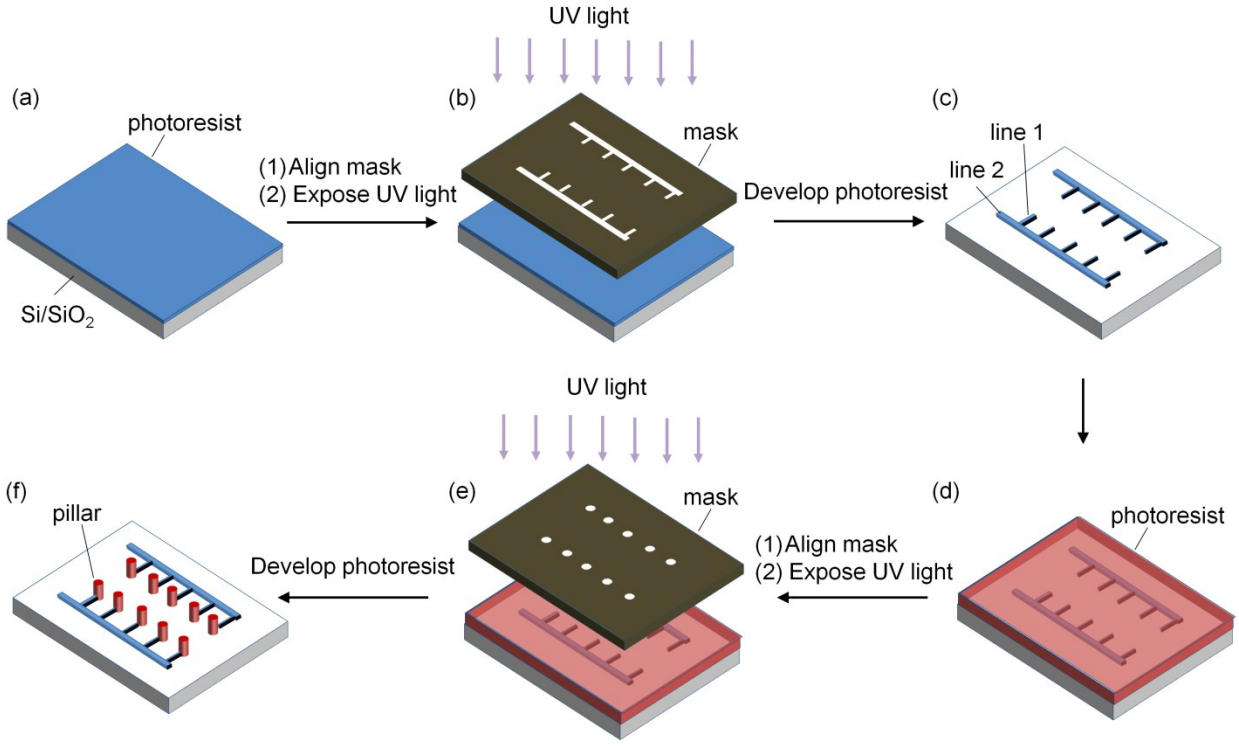

Preparation of PDMS channels 1. A mold which consisted of SU8-3050 photoresist with the dimensions of 0.3 cm × 100 μm × 120 μm, followed by treatment of trichloro(1H,1H,2H,2H-perfluorooctyl)silane (FOTS) vapor in a vacuum dessicator for 30 minutes. To form the PDMS channels, we poured a mixture of 14:1 PDMS and curing agent (Sylgard® 184 silicone elastomer kit, Dow corning cooperation) on the mold and cured the PDMS at 80 ^{o}C for 20 minutes. After curing, we cut the channels out of the PDMS slab using a razor blade and punched two holes (0.2 cm in diameter) at both ends of the channels prior to the alignment described in the main text.

Functionalization of the top-electrode. We functionalized the PDMS chip with 3-(aminopropyl)triethoxysilane (APTES) prior to the injection of GaO_x/EGaIn before the measurements of $SCH_2PhCCPh(CH_2)_3Fc$SAMs on Au^{TS}. The PDMS chip was cleaned with oxygen-plasma for 5 minutes, followed by the treatment of APTES vapor in a vacuum dessicator for 30 minutes. We found that the functionalization reduces the adhesion between PDMS and the SAM surface and possibly lowers the snap-in force when GaO_x/EGaIn is brought into contact with the molecules. After functionalizing of the PDMS surface with APTES, the water contact angle changed from ~95^{o} to ~55^{o} (Figure S5), confirming the presence of a layer of APTES. Without the functionalization of the PDMS with APTES, we observed that the values of $|J|$ were one to two orders of magnitude higher (and the junctions did not rectify; $R = 0.9 \pm 1.3$) at -1.0 V than the values measured by using the APTES modified PDMS devices (Figure S6). We did not observe a significant difference in $|J|$ when measuring junctions with n-alkanethiolate SAMs using the APTES functionalized PDMS devices or devices with native PDMS.

We used APTES-functionalized PDMS top-electrodes to form 15 non-shorting junctions on two different substrates of $SCH_2PhCCPh(CH_2)_3Fc$ SAMs on Au^{TS} (yield = 75%, $N = 600$).

The electrical characteristics of $SCH_2PhCCPh(CH_2)_3Fc$ junctions are shown in the main text (Figure 6d, e and f). The statistics of the electrical measurements of $SC(PhC)_2C_3Fc$ SAMs are summarized in Table S1.

Figure S5. Photograph of a water droplet on (a) PDMS surface and (b) APTES functionalized PDMS surface. The contact angles were ~95° and 55° for images of (a) and (b), respectively.

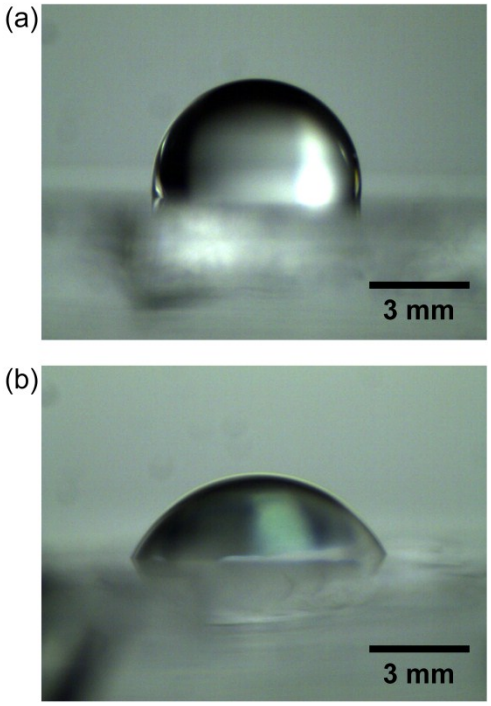

Figure S6. The log average *J*(V) curves of junctions with $SCH_2PhCCPh(CH_2)_3Fc$ SAMs measured by using top-electrodes with top-electrodes with native PDMS (i.e., without functionalization of APTES). The inset shows the histogram of *R* with Gaussian fit to this histogram.

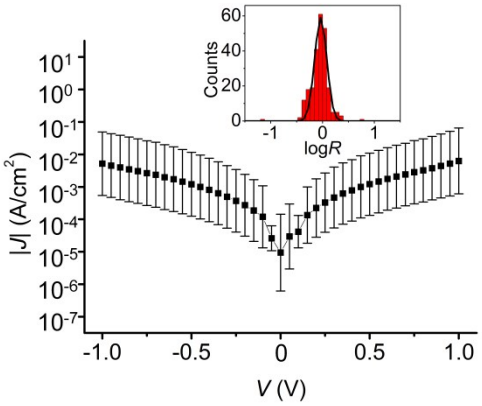

Topography and surface roughness of the bottom-electrode. Figures S7a and S7b show typical AFM images of the Ag^{TS} and Au^{TS} surfaces prepared by template-stripping, respectively.

Table S1. Statistics for electrical measurements of junctions with $SCH_2PhCCPh(CH_2)_3Fc$ SAMs. The *J*(V) curves measured with the PDMS surface of the top-electrodes functionalized with APTES and without APTES are shown in Figure 4d and Figure S6, respectively.

top-electrodes	junctions	non-shorting junctions	yield (%)[a]	*N*[b]	Rectification (*R*)
PDMS surface functionalized with APTES	20	15	75	600	45
PDMS without APTES	20	12	60	480	0.9

[a]The yield of non-shorting junctions,
[b]The number of total *J*(V) traces.

Figure S7. AFM image of (a) a Ag^{TS} surface from which we determined a rms roughness of 0.6 nm and (b) a Au^{TS} surface with a rms roughness of 0.3 nm, both measured over an area of 1 × 1 μm^2.

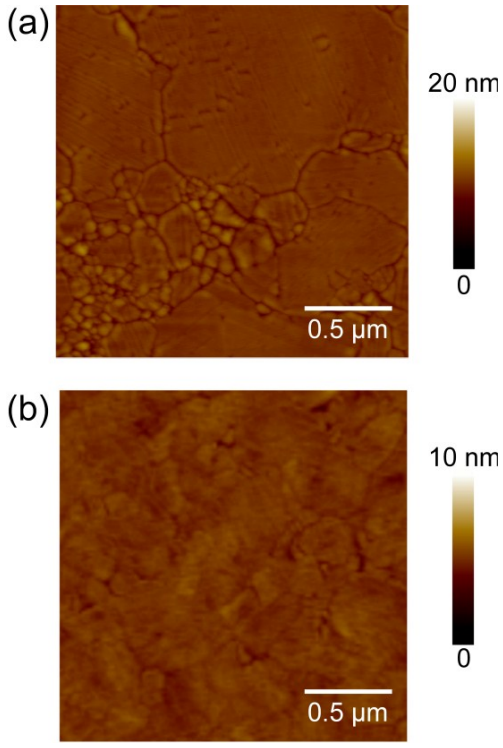

Electrical characteristics and stabilities of the junctions. We collected statistically large numbers of data for junctions with different n-alkanethiolate SAMs by using three different top-electrodes (1560-1640 J(V) curves for each electrode, see Table 1) and obtained the values of $<\log_{10}|J|>_{G,1}$, $<\log_{10}|J|>_{G,2}$, $<\log_{10}|J|>_{G,3}$, $\sigma_{\log,1}$, $\sigma_{\log,2}$ and $\sigma_{\log,3}$ by fitting the histograms of $\log_{10}|J|$ at -0.50 V to Gaussians; the results are shown in Table S2. Figure S8 shows the histograms of $\log_{10}|J|$ at -0.50 V and +0.50 V obtained for all data measured by three different top-electrodes along with Gaussian fits to these histograms (solid lines). Figures S9-S13 show the histograms of $\log_{10}|J|$ at -0.50 V and +0.50 V measured by each top-electrode. Figure S14 shows the stability

tests conducted by sweeping the bias between -0.50 and 0.50 V for 3000 times for devices incorporating $S(CH_2)_9CH_3$, $S(CH_2)_{13}CH_3$ and $S(CH_2)_{17}CH_3$ SAMs.

Table S2. The values of $<\log_{10}|J|>$ and σ_{log} at -0.50 V measured by three different top-electrodes for n-alkanethiolate-based junctions

	top-electrode 1		top-electrode 2		top-electrode 3		Reference values[a]
molecule	$<\log_{10}\|J\|>_{G,1}$	$\sigma_{log,1}$	$<\log_{10}\|J\|>_{G,2}$	$\sigma_{log,2}$	$<\log_{10}\|J\|>_{G,3}$	$\sigma_{log,3}$	$<\log_{10}\|J\|>_{G}$
$S(CH_2)_9CH_3$	-2.01	0.27	-1.96	0.19	-2.07	0.10	-1.7 ± 0.4
$S(CH_2)_{11}CH_3$	-2.91	0.07	-2.79	0.10	-2.51	0.17	-2.4 ± 0.6
$S(CH_2)_{13}CH_3$	-3.68	0.11	-3.73	0.15	-3.42	0.17	-3.2 ± 0.6
$S(CH_2)_{15}CH_3$	-4.47	0.17	-4.52	0.26	-4.48	0.18	-4.2 ± 0.6
$S(CH_2)_{17}CH_3$	-5.38	0.11	-5.35	0.15	-5.39	0.18	-5.0 ± 0.6

[a] The reference values of $<\log_{10}|J|>_G$ were taken from reference 6.

Figure S8. Histograms of $\log_{10}|J|$ at (a) -0.50 V and (b) +0.50 V for junctions with $SC_{n-1}CH_3$ SAMs with n = 10, 12, 14, 16, and 18, with Gaussians fits to the histograms.

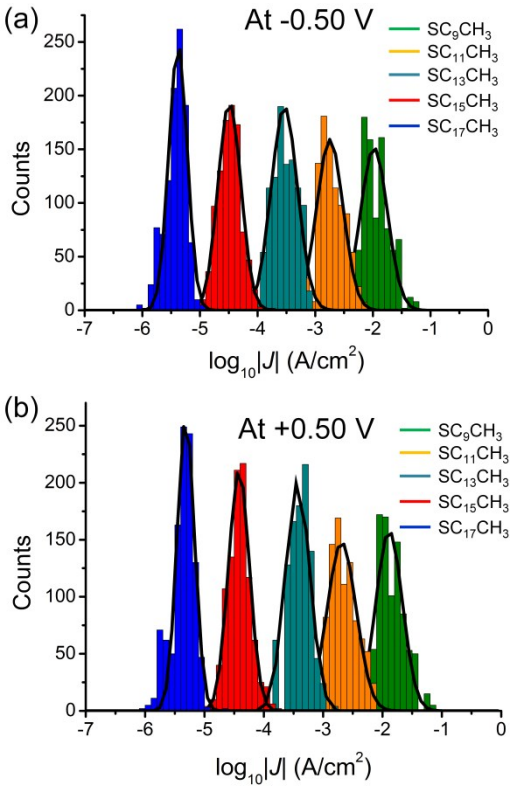

Figure S9. Histograms of $\log_{10}|J|$ at (a)-(c) -0.50 V and (d)-(f) +0.50 V for junctions with $S(CH_2)_9CH_3$ SAMs using three different top-electrodes. The histograms $\log_{10}|J|$ measured by each top-electrode are superimposed on the histograms of all data.

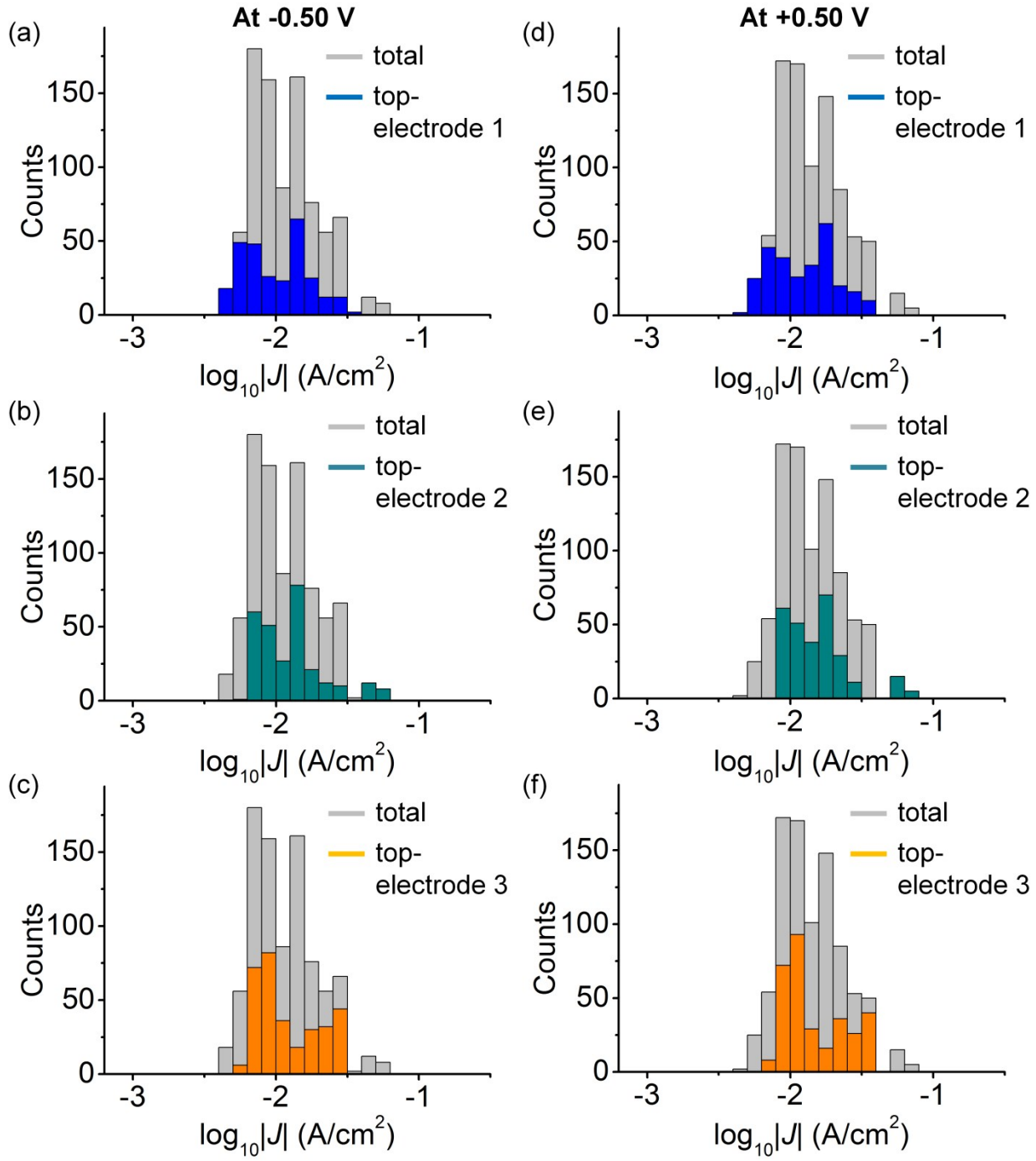

Figure S10. Histograms of $\log_{10}|J|$ at (a)-(c) -0.50 V and (d)-(f) +0.50 V for junctions with $S(CH_2)_{11}CH_3$ SAMs using three different top-electrodes. The histograms $\log_{10}|J|$ measured by each top-electrode are superimposed on the histograms of all data.

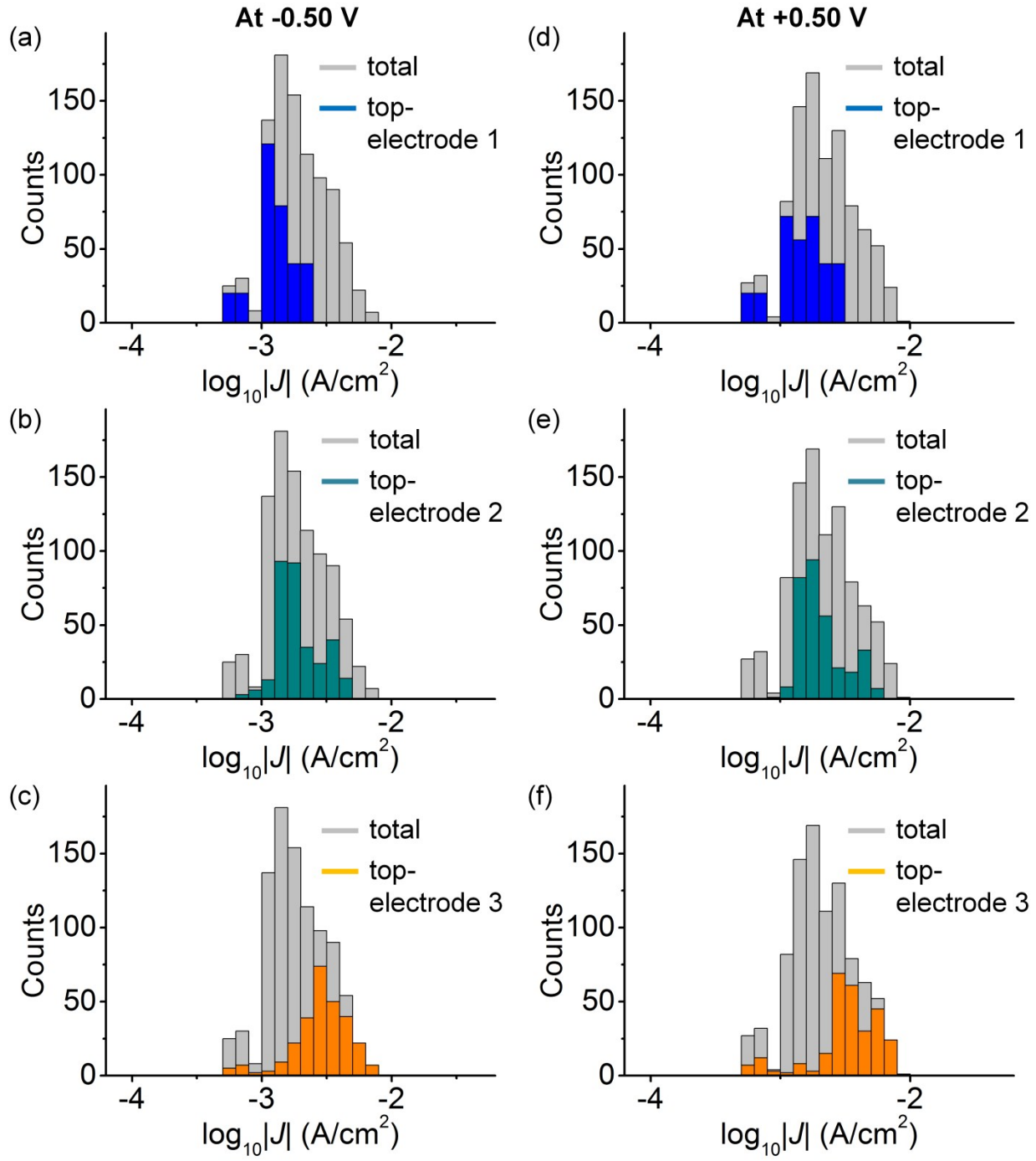

Figure S11. Histograms of $\log_{10}|J|$ at (a)-(c) -0.50 V and (d)-(f) +0.50 V for junctions with $S(CH_2)_{13}CH_3$ SAMs using three different top-electrodes. The histograms $\log_{10}|J|$ measured by each top-electrode are superimposed on the histograms of all data.

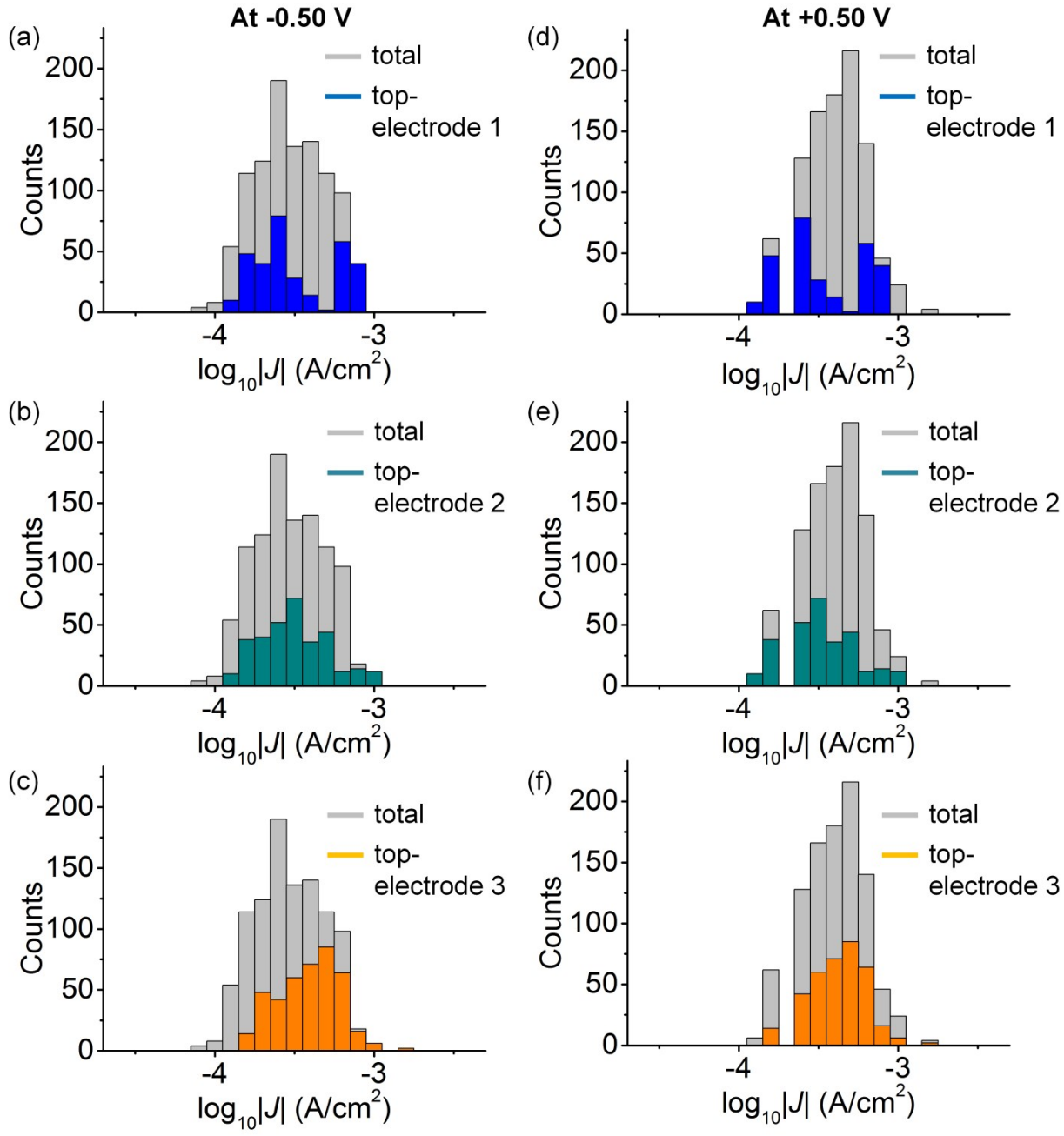

Figure S12. Histograms of $\log_{10}|J|$ at (a)-(c) -0.50 V and (d)-(f) +0.50 V for junctions with $S(CH_2)_{15}CH_3$using three different top-electrodes. The histograms $\log_{10}|J|$ measured by each top-electrode are superimposed on the histograms of all data.

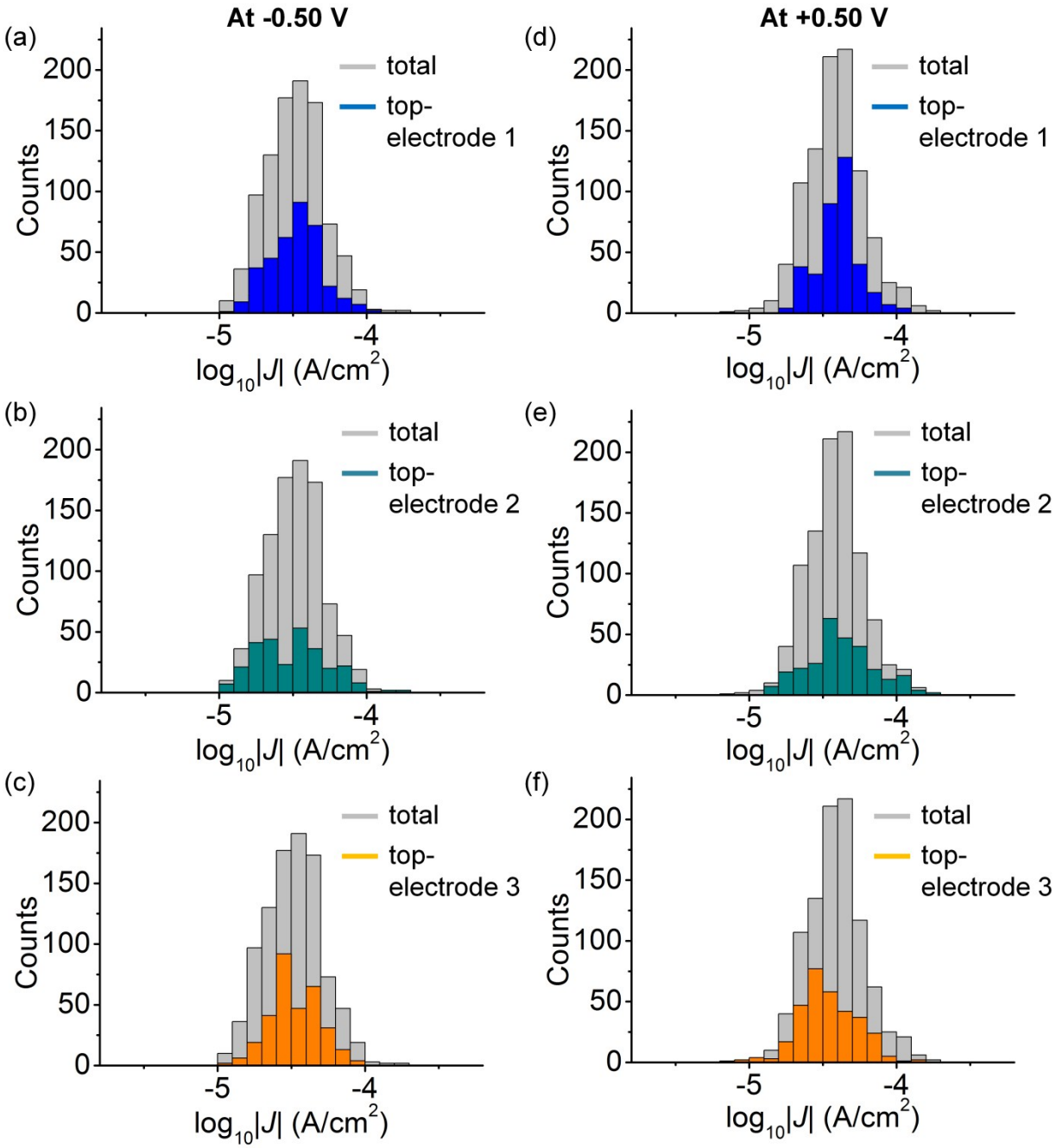

Figure S13. Histograms of $\log_{10}|J|$ at (a)-(c) -0.50 V and (d)-(f) +0.50 V for junctions with $S(CH_2)_{17}CH_3$ SAMs using three different top-electrodes. The histograms $\log_{10}|J|$ measured by each top-electrode are superimposed on the histograms of all data.

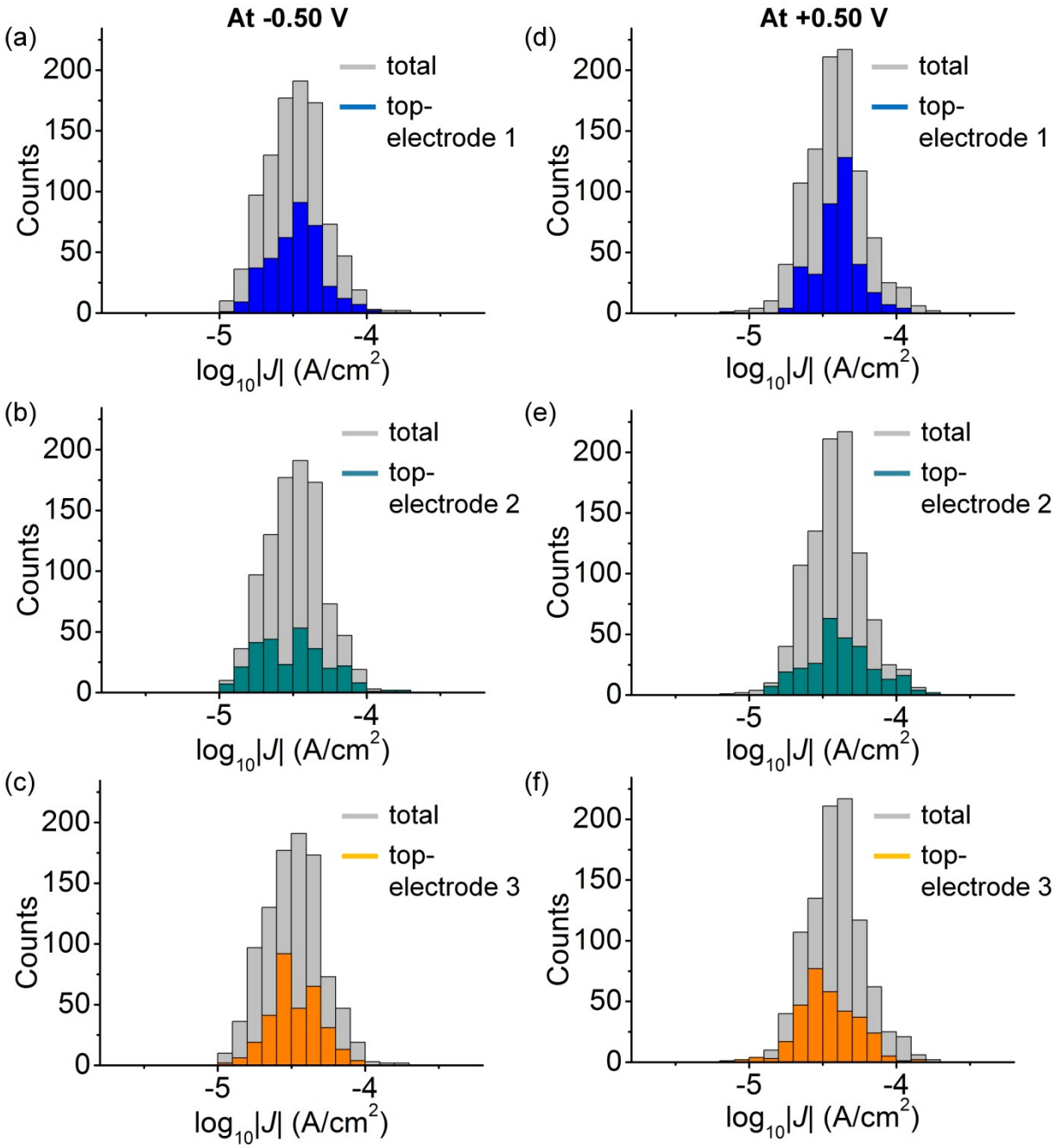

Figure S14. 3000 *J*(V) curves for junctions of $S(CH_2)_9CH_3$, $S(CH_2)_{13}CH_3$ and $S(CH_2)_{17}CH_3$ measured by continuous sweeping the bias between -0.50 and 0.50 V.

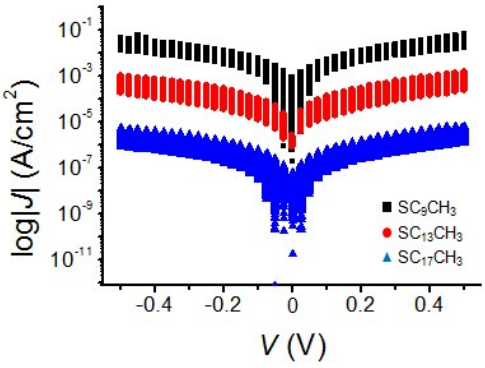

The fabrication of junctions with a patterned Ag^{TS} bottom-electrode. We used strips of Scotch tape (Scotch^R Magic^{TM} from 3M) as the shadow mask which was placed in direct contact with the silicon wafer. We evaporated a layer of Ag as described in experimental section and then peeled off the tape carefully. The template-stripping procedure was the same as described before, but prior to deposition of the optical adhesive (OA), the Si/SiO_2 was functionalized with tridecafluoro-1,1,2,2-tetrahydrooctyltrichlorosilane (FOTS) to minimize the adhesion of the OA with the Si/SiO_2 (as has been described in ref 7). The formation of the SAM and experimental methods of the charge transport measurements and data analysis were the same as described above.

Figure S15. A) Photograph of a complete device with a patterned Ag^{TS} bottom-electrode. B) AFM image of the patterned Ag^{TS} surface with a rms roughness of 0.4 nm measured over an area of 2 × 2 μm^2. C) Plot of the average $\langle \log_{10}|J| \rangle_G$ vs. applied bias for junctions with SC_{14} SAMs. The error bars represent log-standard deviations from 50 traces.

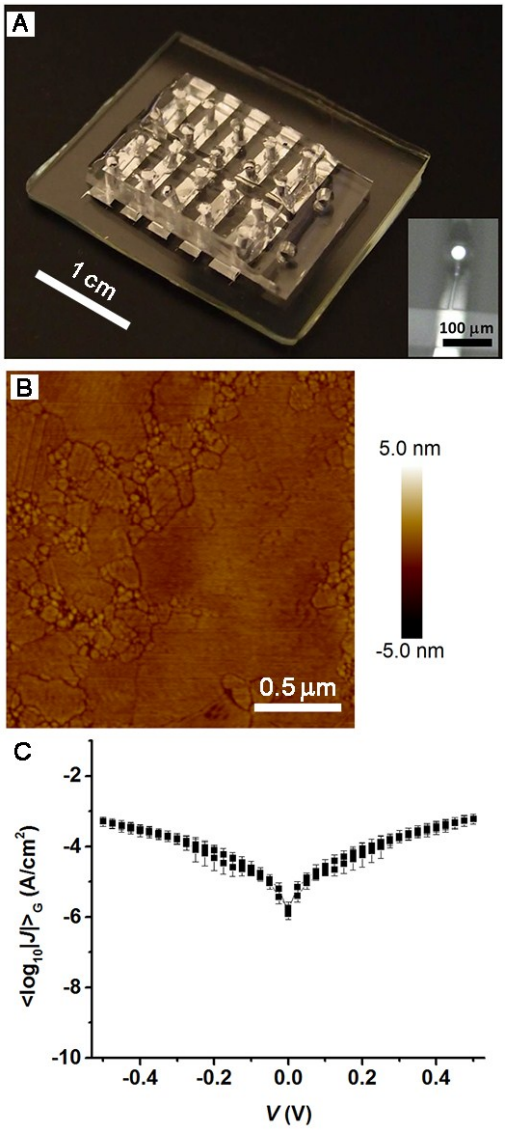

References

[1] L. Yuan, N. Nerngchamnong, L. Cao, H. Hamoudi, E. Del Barco, M. Roemer, R. Sriramula, D. Thompson, C. A Nijhuis, *Nat. Commun.* 2015, **6**, Article number: 6324.
[2] L. J. Wang, L. Yuan, C. A. Nijhuis. *Manuscript in preparation*.
[3] C. Vericat, M. E. Vela, G. Corthey, E. Pensa, E. Cort´es, M. H. Fonticelli, F. Ibanez, G. E. Benitez, P. Carro and R. C. Salvarezza, *RSC Adv*., 2014, **4**, 27730-27754
[4] ISO, 1994 Replicability (Trueness and Precision) of Measurement Methods and Results: General Principles and Definitions/Part 1, International Organization for Standardization Geneva, Switzerland.
[5] E. P. Kartalov, C. Walker, C. R. Taylor, W. F. Anderson and A. Scherer, *P. Natl. Acad. Sci.USA* 2006, **103**, 12280-12284.
[6] A. Wan, J. Li, C. S. Suchand Sangeeth and C. A. Nijhuis, *Adv. Func. Mater*., 2014, **24**, 4442-4456.
[7] C. A. Nijhuis, W. F. Reus, M. D. Dickey and G. M. Whitesides. *Nano Lett.* 2010, **10**, 3611.